Received: 15 November 2018 | Revised: 2 April 2019 | Accepted: 4 April 2019

DOI: 10.1111/ter.12398

SPECIAL ISSUE - THERMO2018

Terra Nova WILEY

Differential uplift on the boundary between the Eastern and the Southern European Alps: Thermochronologic constraints from the Brenner Base Tunnel

Thomas Klotz[1] | Hannah Pomella[1] | Martin Reiser[2] | Bernhard Fügenschuh[1] | Massimiliano Zattin[3]

[1]Department of Geology, University of Innsbruck, Innsbruck, Austria

[2]Geological Survey of Austria, Vienna, Austria

[3]Department of Geosciences, University of Padova, Padova, Italy

Correspondence
Thomas Klotz, Department of Geology, Universitat Innsbruck, Innrain 52f, A6020 Innsbruck, Tirol 6020, Austria.
Email: thomas.klotz@student.uibk.ac.at

Funding information
University of Innsbruck

Abstract

The Brenner Base Tunnel will connect Innsbruck (Austria) and Franzensfeste (Italy) by piercing two of the most important fault structures of the Alps: the Periadriatic fault system (PFS) and the Southern limit of Alpine metamorphism (SAM). (U-Th)/He dating (apatite) and fission-track analysis (apatite and zircon) on samples taken during excavation reveal a complex pattern of exhumation through time. The results yield temporal constraints for relative vertical block movement and fault activity. Furthermore, they indicate differential uplift of the northern block along the ~E–W striking PFS and allow locating the position of the SAM in the overtilted nappe stack south of the Tauern Window. Our data strongly support, for the first time, an ongoing north-side-up movement along this section of the PFS until at least the end of Miocene.

1 | INTRODUCTION

The excavation of the Brenner Base Tunnel provides a unique opportunity to sample a section at almost constant elevation across the Adria-Europe collision zone in the Eastern Alps (Figure 1). It crosscuts complex Alpine structures such as the Tauern Dome, which is overlain by the Austroalpine nappe stack, and the southward adjacent Periadriatic fault system (PFS), a first-order tectonic boundary separating Eastern and Southern Alps (Bögel, 1975; Frisch, Kuhlemann, Dunkl, & Brügel, 1998; Laubscher, 1971; Schmid, Aebli, & Zingg, 1989; Werling, 1992).

During the Alpine orogeny (a) Cretaceous nappe stacking (Froitzheim, Schmid, & Frey, 1996; Thöni & Jagoutz, 1993) and associated metamorphism affected the Austroalpine domain, followed by (b) extension and reorganization, post-dating Eoalpine lithospheric thickening (Froitzheim, Schmid, & Conti, 1994), (c) Penninic subduction during Adria-Europe convergence and (d) collision of continental, crustal blocks. Large-scale Alpine structures formed as a consequence of crustal shortening during the late-orogenic, post-collisional Neoalpine (Trümpy, 1973) indentation of the Adriatic microplate from latest Eocene onwards (Froitzheim et al., 1994; Ratschbacher, Frisch, Linzer, & Merle, 1991).

Evidence for all these orogenic stages persists in a narrow corridor near Mauls (Italy), pierced by the tunnel close to its southern portal (Figure 1). We derived low-temperature radiometric ages for a transect comprising, from north to south, (a) subvertical to partly overtilted Austroalpine nappes on the southern limb of the western Tauern sub-dome (Rosenberg et al., 2018), (b) Periadriatic intrusive rocks bound by branches of the PFS (both north and south) and (c) Southalpine Permian intrusion.

During ongoing Neoalpine convergence, severe pinching of the units north of the PFS between the upfolded Tauern Window and

This paper was presented at the 16th International Conference on Thermochronology (Quedlinburg, Germany, September 2018).

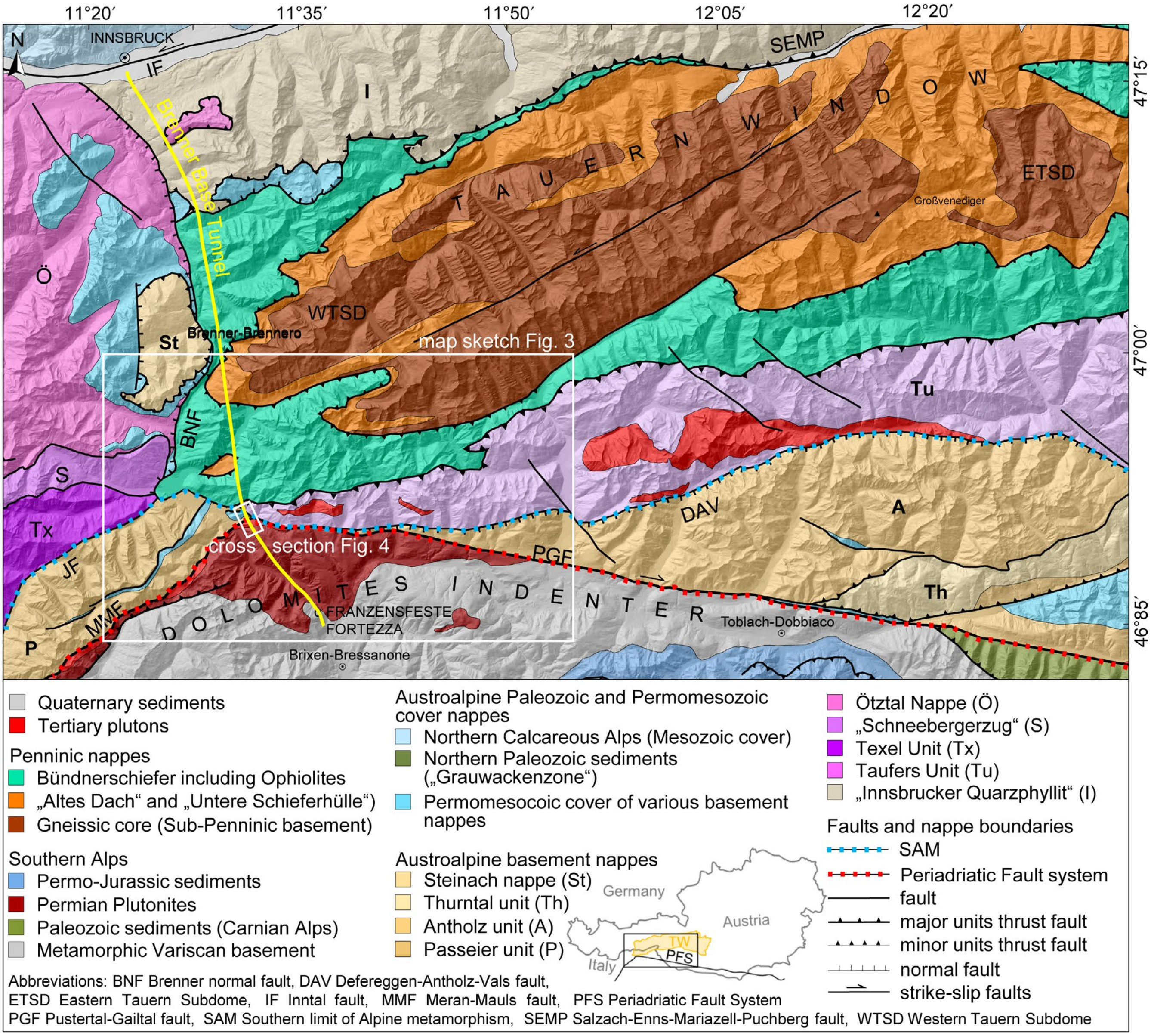

FIGURE 1 Geological overview along the trace of the Brenner Base Tunnel, crosscutting the Tauern Window and the border between Eastern and Southern Alps. The examined cross section (position indicated by the small white rectangle) pierces both DAV and PFS. The map is based on the ‘Geological Overview’, compiled by the ‘Amt für Geologie und Baustoffprüfung der Südtiroler Landesverwaltung’, which is derived from published and still unpublished findings of the projects ‘CARG’ and ‘Basiskarte’ as well as existing Italian and Austrian geological maps and the ‘Geologische Übersichtskarte von Tirol’ (Brandner, 1980) [Colour figure can be viewed at wileyonlinelibrary.com]

the northern tip of the indenting Adriatic crust resulted in their thinning due to lateral extrusion (Ratschbacher et al., 1991) as well as vertical extension. This study aims at localizing major boundaries between blocks of coherent exhumation behaviour and at constraining the timing of their vertical displacement.

2 | GEOLOGICAL SETTING

During the Cenozoic orogeny, the Tauern Dome—comprising nappes derived from the distal European margin and ophiolite-bearing Penninic nappes—formed as a consequence of (micro-) plate convergence and crustal accretion in a N–S compressional setting (Frisch et al., 1998; Lammerer, 1988; Linzer, Decker, Peresson, Dell'Mour, & Frisch, 2002; Schmid, Scharf, Handy, & Rosenberg, 2013). Major exhumation from Eocene onward is accommodated in structures related to this shortening, such as the Venediger Duplex (Frisch, 1977; Frisch et al., 1998; Lammerer & Weger, 1998), the top-to-north directed Sub-Tauern Ramp (TRANSALP Working Group, 2002, correction published 2006) and associated thrusts (Ortner, Reiter, & Brandner, 2006).

The Austroalpine nappe stack overlies the Penninic and Sub-Penninic units (Reiter et al., 2018, the tunnel cross section presented coincides with the trace of their figure 8). Austroalpine

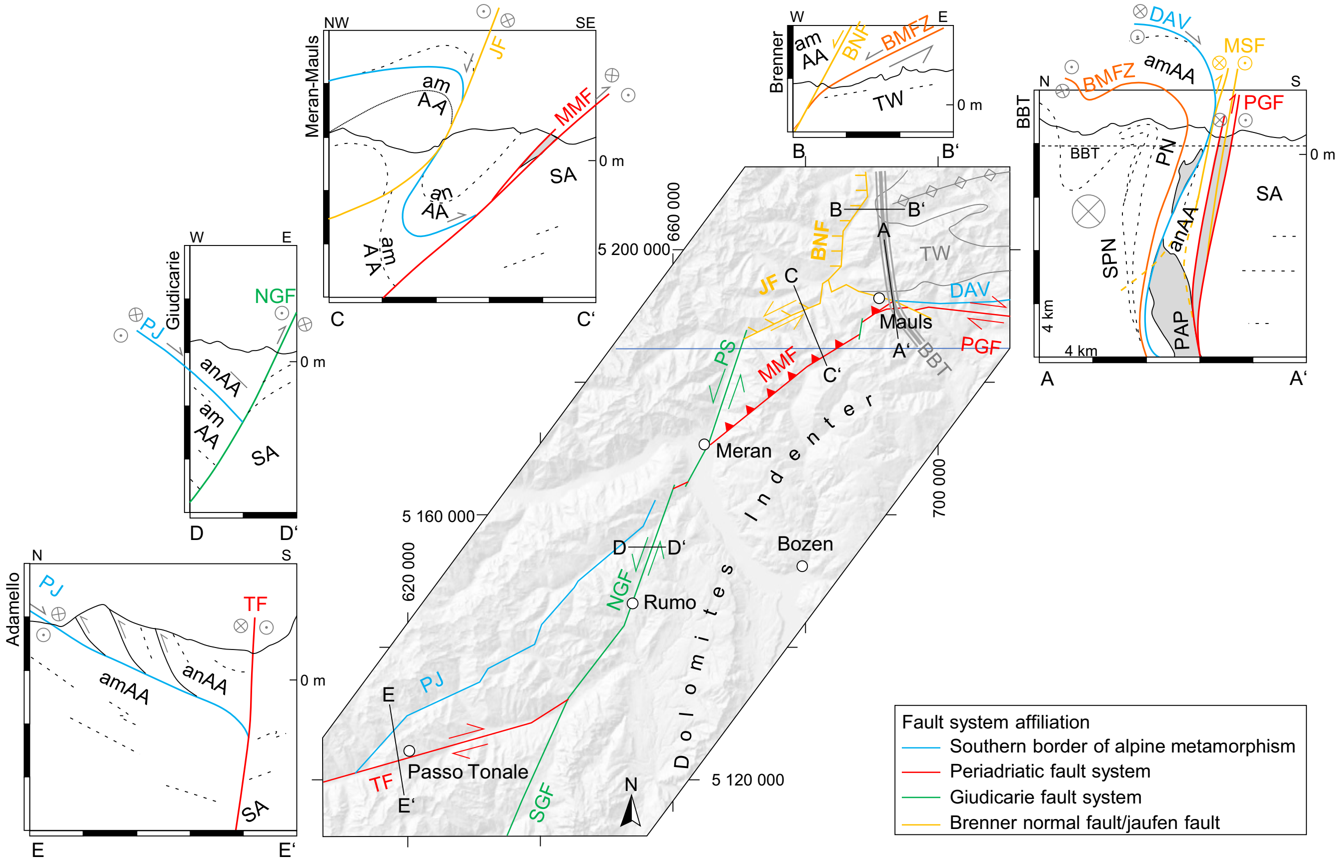

FIGURE 2 Simplified map and cross sections of the Periadriatic fault system between Passo Tonale (W) and the western part of the Tauern Window (E), based on Pomella et al. (2012); The colour code indicates the tectonic affiliation of single faults to superordinate fault systems. Cross sections modified based on: (A–A′) Reiter et al. (2018), (B–B′) Selverstone (1988), (C–C′ and D–D′) Pomella, Flöss, Speckbacher, Tropper, and Fügenschuh (2016), (E–E′) Viola, Mancktelow, Seward, Meier, and Martin (2003); one segment of the cross-sectional scale bar equals 4 km; amAA, Alpine metamorphic Austroalpine units; anAA, Alpine non-metamorphic Austroalpine units; BNF, Brenner normal fault; BMFZ, Brenner mylonitic fault zone; DAV, Defereggen-Antholz-Vals fault; JF, Jaufen fault; MMF, Meran-Mauls fault; MSF, Mauls-Sprechenstein fault zone; NGF, Northern Giudicarie fault; PGF, Pustertal-Gailtal fault; PJ, Pejo fault; PN, Penninic nappes; PS, Passeier fault; SA, Southalpine units; SGF, Southern Giudicarie fault; SPN, Sub-Penninic nappes; TF, Tonale fault; TW, Tauern Window [Colour figure can be viewed at wileyonlinelibrary.com]

FIGURE 3 Schematic cross section (a) and map view (b) for the investigated area between the southern limb of the western Tauern sub-dome and Southalpine units, both showing main tectonic boundaries and thrusts in the survey area east of the Giudicarie belt; indication of map extent see Figure 1; (c) structural map of the study area with main faults; Abbreviations see Figure 2; SN, Senges normal fault [Colour figure can be viewed at wileyonlinelibrary.com]

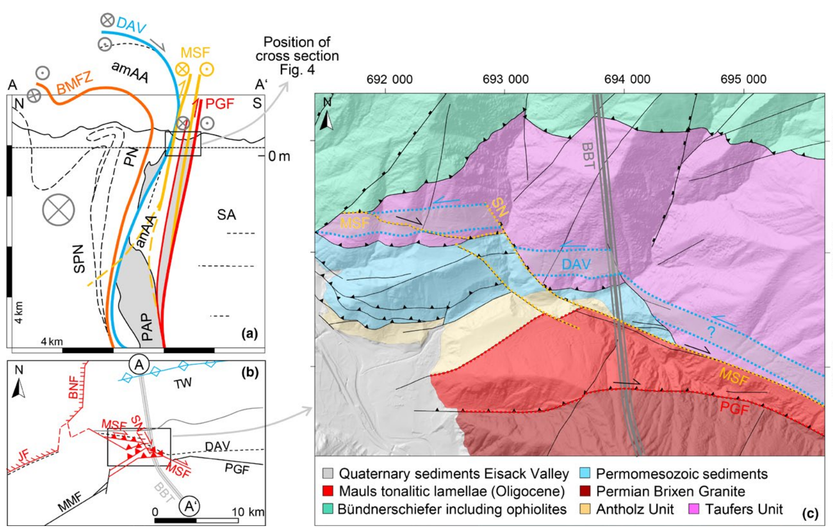

units can be subdivided into a northern part affected by Eoalpine metamorphism (lower nappes during orogeny) which was juxtaposed to a weakly to non-affected (uppermost nappes) southern one (Borsi, Moro, & Ferrara, 1972) by a set of faults (Figure 2, blue) that mark the 'Southern limit of Alpine metamorphism' (SAM, Hoinkes et al., 1999). This tectonic structure is attributed to post-Eoalpine, latest Cretaceous to Paleogene extension (Froitzheim et al., 1994; Fügenschuh, 1995). In the investigated area, the SAM spatially coincides with the Defereggen-Antholz-Vals fault zone (DAV, Hoinkes et al., 1999), is in steep orientation and incorporated in the southern limb of the western Tauern sub-dome.

South of the westernmost Tauern Window, Zircon fission-track data indicate (a) Lower Cretaceous to early Oligocene cooling for Austroalpine samples south of the DAV and (b) Oligocene to middle Miocene cooling for those north of the DAV. (c) Miocene cooling ages cluster in the adjacent Penninic and Sub-Penninic units, north of the southern boundary of the Tauern Window (Bertrand, Rosenberg, Rabaute, Herman, & Fügenschuh, 2017).

Samples from the Austroalpine domain show Apatite fission-track ages between Oligocene and middle Miocene. Middle to late Miocene ages are observed within the Tauern Window (Luth & Willingshofer, 2008; Rosenberg et al., 2018). This pattern indicates the Miocene exhumation process of the Tauern Dome and proves earlier cooling of its overlying, Austroalpine thrust sheet, framing the Tauern Window today. It is remarkable that the SW part of the Austroalpine domain, marked as Passeier unit in Figure 1, shows more affinity to the Tauern Window than to its eastern continuation in both Apatite and Zircon fission-track age pattern (Bertrand et al., 2017).

The PFS (Figure 2), decoupling the Austroalpine nappe stack from the Southalpine domain (Adriatic Indenter), is a first-order structural element of the Alpine orogen (Handy, Schmid, Bousquet, Kissling, & Bernoulli, 2010; Schmid et al., 1989). The formerly straight, ~W–E trending PFS was active as a dextral strike-slip fault at least until 31–28 Ma (Handy, Ustaszewski, & Kissling, 2015; Pomella, Klötzli, Scholger, Stipp, & Fügenschuh, 2011; Schneider et al., 2015). A different initial setting with a curved (restraining bend) PFS is discussed by Viola, Mancktelow, and Seward (2001). Differential Adriatic indentation, initiated in the late Oligocene and mainly accommodated by the sinistral Giudicarie Fault system (GFS, Pomella et al., 2011), offsets the PFS and dissects the indenter in a western and an eastern (Dolomites Indenter) segment (Rosenberg, Brun, Cagnard, & Gapais, 2007). Miocene offset along the GFS is verified by Pleuger, Mancktelow, Zwingmann, and Manser (2012) who dated fault gouge along the Northern Giudicarie fault to

TABLE 1 Sample coordinates, apatite and zircon fission-track analytical data from tunnel cross section

Sample ID		Position in tunnel			Coordinates			BBT-TM Coord.		Zircon				
Name	Source	Tunnel S [m]	Tunnel N [m]	Source [m]	UTM N	UTM E	z [m]	x [m]	y [m]	Nb	Nd	ρD [10^5 cm^{-2}]	Ns	ρs [10^5 cm^{-2}]
PK1	EKS Periadriatica	10,990	48,314	–	5,191,703	694,417	718	21,656	85,511	10	3,062	4.9	1,416	266.757
PK2	EKS Periadriatica	11,020	48,284	–	5,191,733	694,412	718	21,652	85,540	22	3,062	4.7	2,607	267.887
PK3	EKS Periadriatica	11,082	48,222	–	5,191,794	694,402	719	21,644	85,602	–	–	–	–	–
PK5	EKS Periadriatica	11,140	48,164	–	5,191,851	694,393	719	21,636	85,659	42	3,062	4.6	4,045	57.470
HTW-48050	Haupttunnel W	11,254	48,050	–	5,191,960	694,340	732	21,587	85,769	20	3,800	5.0	384	46.647
HTE-47865	Haupttunnel O	11,439	47,865	–	5,192,151	694,380	732	21,633	85,959	–	–	–	–	–
HTW-47834	Haupttunnel W	11,470	47,834	–	5,192,173	694,305	733	21,560	85,984	22	3,800	5.0	774	53.006
HTW-47650	Haupttunnel W	11,654	47,650	–	5,192,355	694,276	733	21,536	86,166	–	–	–	–	–
SA7CC-006	Vorausb.	11,738	47,567	6	5,192,441	694,298	721	21,561	86,252	14	3,800	5.0	258	40.502
SA7CC-023	Vorausb.	11,755	47,550	23	5,192,458	694,295	721	21,559	86,268	21	3,800	4.0	500	41.820
SA7CC-065	Vorausb.	11,797	47,508	65	5,192,499	694,288	721	21,553	86,310	8	3,800	5.0	138	37.057
SA7CC-136	Vorausb.	11,868	47,437	136	5,192,569	694,277	722	21,544	86,380	11	3,800	4.0	290	43.517
SA7CC-157	Vorausb.	11,889	47,416	157	5,192,590	694,274	722	21,542	86,401	12	3,800	4.0	314	31.108
SA7CC-247	Vorausb.	11,979	47,326	247	5,192,679	694,260	722	21,530	86,491	21	3,800	4.0	981	131.713
SA7CC-320	Vorausb.	12,052	47,253	320	5,192,751	694,248	722	21,521	86,563	5	3,800	5.0	358	228.316
SAV11-8	Vorausb. SAV11	12,183	47,121	8	5,192,881	694,227	723	21,504	86,694	21	3,016	3.3	1,626	68.071
SAV11-44	Vorausb. SAV11	12,219	47,085	44	5,192,917	694,221	723	21,500	86,730	5	3,016	3.0	245	20.944
SAV11-84	Vorausb. SAV11	12,259	47,045	84	5,192,956	694,215	723	21,494	86,769	14	3,016	3.7	655	29.747
SAV20-42	Vorausb. SAV20	12,428	46,877	42	5,193,122	694,188	724	21,473	86,936	42	3,016	3.4	2,316	22.633
SAV20-49	Vorausb. SAV20	12,435	46,870	49	5,193,129	694,187	724	21,472	86,943	–	–	–	–	–
SAV20-74	Vorausb. SAV20	12,460	46,845	74	5,193,154	694,183	724	21,469	86,968	6	3,016	3.1	249	20.934

Abbreviations: ρD, track density of the dosimeter glass; ρs, spontaneous track density; ρi, induced track density; χ, chi-square statistics; Nb, number oc crystals; P, processor zeta value (ζ apatite/ ζ zircon): 1 (349 ± 29/ 154 ± 7), 2 (318 ± 27/ 130 ± 10), 3 (337 ± 25/ 190 ± 11);U-galsses used: CN1 (zircon), CN5 (apatite)

~17 Ma. The segment of the PFS pierced by the Brenner Base Tunnel just east of the GFS is termed Pustertal-Gailtal fault (PGF). The faults in Figure 2 are colour-coded due to their tectonic affiliation to one of the following systems: SAM, PFS, GFS, Brenner normal fault/Jaufen fault.

The numerous magmatic bodies exposed along the PFS (Figure 1; see Pomella et al., 2011, their figure 6 for a complete compilation) are collected under the term 'Periadriatic intrusions' (Becke, 1903; Bianchi, Callegari, & Jobstraibizer, 1970; Dal Piaz, 1926, 1942; Deutsch, 1984; Rosenberg, 2004; Sassi & Zanferrari, 1971; , 1973; von Blanckenburg et al., 1998). While these intrusions formed from 36 to 29 Ma (Pomella et al., 2011 and citations therein), only the mafic southwestern intrusive bodies of the Adamello batholite date back to 43 Ma (Hansmann & Oberli, 1991). In the study area the Periadriatic intrusions are represented by the Mauls lamellae (32–33 Ma; Pomella et al., 2011) which is bounded by faults on all sides (Figures 1 and 3): the Meran-Mauls fault (MMF) to the NW, the PGF to the south and the Mauls-Sprechenstein fault system (MSF) to the NE (Brandner, Reiter, & Töchterle, 2008). The latter is characterized as a dextral fault including a transpressional stepover (Bistacchi, Massironi, & Menegon, 2010) near Mauls. Stöckli (1995) mapped a dissection of the MSF by east dipping normal faults (e.g. Senges normal fault).

The Brixen Pluton (Rottura et al., 1998; Thöny, 2008), a Permian granitic intrusion (279 ± 7 Ma, Thöny, 2008), represents the Southalpine domain in the study area.

3 | METHODOLOGY

Fission-track analysis is based on the spontaneous fission of ^{238}U while the associated formation of latent destruction trails in solid media (Wagner & van den Haute, 1992). Apatite (AFT) and zircon (ZFT) preserve these tracks at temperatures below 60°C and 180°C respectively (Donelick, Carlson, & Ketcham, 1999; Hurford & Green, 1983) for geologically significant time scales. Above these temperatures, fission tracks shorten in a time- and temperature-dependent manner within the partial annealing zone (Carlson, Donelick, & Ketcham, 1999).

(U-Th)/He on apatite (AHe) allows for dating of rock cooling below 60–70°C (Wolf, Farley, & Silver, 1996), as He diffuses and abandons the system at temperatures higher than 80°C and remains quantitatively steady below 40°C.

Thermal histories of the samples were modelled using the HeFTy® modelling software (Ketcham, 2005) and the annealing model of Ketcham, Carter, Donelick, Barbarand, and Hurford (2007). Dpar

					Apatite										
Ni	ρi [10^5 cm^2]	χ [%]	Age ± 1σ	P	Nb	Nd	ρD [10^5 cm^{-2}]	Ns	ρs [10^5 cm^2]	Ni	ρi [10^5 cm^2]	χ [%]	Age ± 1σ	P	Dpar [μm]
379	71.399	74.18	140.60 ± 10.40	1	21	3,100	13.6	52	0.933	836	14.993	100.00	14.30 ± 2.30	3	–
759	77.993	40.59	123.80 ± 7.60	1	13	3,100	13.5	39	1.290	438	14.488	84.75	20.20 ± 3.70	3	–
–	–	–	–		20	3,100	13.4	62	1.302	836	17.552	99.78	16.80 ± 2.60	3	1.70
6,212	88.260	0.00	23.40 ± 1.30	1	16	3,100	13.0	70	2.314	1,624	53.675	72.26	9.40 ± 1.40	3	–
561	68.149	50.73	21.00 ± 1.80	2	17	4,000	12.0	210	4.730	3,801	85.620	34.25	10.60 ± 1.20	2	1.73
–	–	–	–		21	3,100	13.8	241	2.617	4,246	46.099	39.84	13.10 ± 1.30	3	–
899	61.567	41.39	26.40 ± 1.90	2	21	4,000	12.0	260	4.002	4,112	63.285	39.15	12.20 ± 1.30	2	1.86
–	–	–	–		14	3,100	13.0	135	3.963	2,465	72.366	18.14	12.10 ± 1.60	3	–
372	58.399	89.47	21.30 ± 2.00	2	20	4,000	13.0	139	5.837	1,715	72.016	97.37	16.80 ± 2.00	2	–
636	53.195	73.93	19.40 ± 1.60	2	19	4,000	13.0	133	5.301	1,665	66.366	95.48	16.50 ± 2.00	2	1.50
149	40.011	28.90	28.80 ± 4.20	2	–	–	–	–	–	–	–	–	–		–
295	44.268	3.51	23.80 ± 3.00	2	–	–	–	–	–	–	–	–	–		–
312	30.909	58.98	24.70 ± 2.40	2	–	–	–	–	–	–	–	–	–		–
203	27.256	19.91	116.90 ± 11.40	2	–	–	–	–	–	–	–	–	–		–
69	44.005	14.02	156.40 ± 24.50	2	–	–	–	–	–	–	–	–	–		–
1,353	56.642	0.00	29.70 ± 2.60	1	29	3,027	11.0	63	0.420	1,664	11.103	99.58	7.30 ± 1.10	1	1.91
353	30.177	90.97	16.50 ± 0.70	1	18	3,027	11.4	52	0.649	803	10.022	50.82	12.50 ± 2.30	1	1.82
1,109	50.365	22.33	16.80 ± 1.20	1	55	3,027	11.6	208	0.833	4,120	16.497	93.00	10.20 ± 1.10	1	1.79
4,613	45.080	0.01	13.20 ± 0.80	1	37	3,027	11.1	62	0.266	1,828	7.836	99.52	6.60 ± 1.00	1	1.82
–	–	–	–		28	3,027	12.0	129	1.335	2,387	24.704	37.02	10.90 ± 1.40	1	1.76
383	32.200	44.52	16.30 ± 1.10	1	24	3,027	11.2	67	0.499	2,311	17.212	99.36	5.70 ± 0.90	1	1.97

values (Donelick, 1993) were included in the modelling as kinematic parameter indicating the chemical composition of the individual grains.

4 | THERMOCHRONOLOGY RESULTS

18 ZFT, 16 AFT (Table 1) and 11 AHe (Table 2) ages were analysed. A statistically reliable number of track lengths in apatite was only obtained from samples HTW-48050 (*n* = 101) and HTW-47834 (*n* = 103). Nevertheless, the low number of track lengths from SAV20-42 (*n* = 34), SA7CC-023 (*n* = 27) still provided good modelling results (radial plots and track length distribution, see Supporting Information). For AHe dating, two to three replicates were dated for each sample and analytical data were in general acceptable, although critically low He concentration (<1 mol/g) occurred in some grains. Given the generally high

TABLE 2 Sample coordinates and (U-Th)/He on apatite analytical data from tunnel cross section

Sample ID		Position in tunnel			Coordinates			BBT-TM Coord.		(U–Th–Sm)/He analysis	
Name	Source	Tunnel S [m]	Tunnel N [m]	Source [m]	UTM N	UTM E	*z* [m]	*x* [m]	*y* [m]	Grain ID	Raw age [Ma]
PK1	EKS Periadriatica	10,990	48,314	—	5,191,703	694,417	718	21,656	85,511	P1	11.28
										P5	18.73
										P8	11.44
PK2	EKS Periadriatica	11,020	48,284	—	5,191,733	694,412	718	21,652	85,540	P1	8.45
										P2	9.96
										P3	9.30
PK3	EKS Periadriatica	11,082	48,222	—	5,191,794	694,402	719	21,644	85,602	P2	20.14
										P3	11.87
										P4	21.93
PK5	EKS Periadriatica	11,140	48,164	—	5,191,851	694,393	719	21,636	85,659	P3	3.65
										P4	1.61
										P8	2.56
PK6	EKS Periadriatica	11,173	48,131	—	694,387	5,191,884	719	21,632	85,692	P4	0.55
										P7	1.52
										P9	1.35
PK7	EKS Periadriatica	11,201	48,103	—	694,383	5,191,912	719	21,629	85,720	P1	1.43
										P2	2.54
										P3	4.90
HTW-48050	Haupttunnel West	11,254	48,050	—	5,191,960	694,340	732	21,587	85,769	1	3.13
										2	4.84
										3	3.63
HTE-47865	Haupttunnel Ost	11,439	47,865	—	5,192,151	694,380	732	21,633	85,959	1.00	4.36
										2.00	3.66
										3.00	2.65
HTW-47834	Haupttunnel West	11,470	47,834	—	5,192,173	694,305	733	21,560	85,984	1.00	2.53
										2.00	3.81
										3.00	3.71
SA7CC-006	Vorausbohrung	11,738	47,567	6	5,192,441	694,298	721	21,561	86,252	1	3.51
										3	1.37
SA7CC-023	Vorausbohrung	11,755	47,550	23	5,192,458	694,295	721	21,559	86,268	1	1.97
										2	2.60

Note: Raw age (±σ): age of the grain before the correction; Radius: radius of a hypothetical sphere that should approximate the crystal. It is calculated as the mean between the two dimensions measured in each single grain; U, Th, Sm (ppm): U, Th and Sm contents; 4He (nmol/g): concentration of He measured by the mass spectrometer; eU (ppm): Effective Uranium, quantity typically used to represent the concentration of U and Th. It is calculated according to the formula: eU=[U] +0.235 × [Th]; FT 238U, 235U, 232Th, 147Sm: alpha-ejection correction factor. The resulting dates require a correction for He loss occurred by ejection of α particles outside the crystal domain; Fully corrected FT age (±σ): age of the grain after the correction.
[a]Calculated with analytical error.

reproducibility of single grains, a weighted mean age was calculated for each sample.

Based on spatial association and similar cooling history, six domains were identified (Figure 4). These 'groups' are briefly described in Table 3 and discussed in the following paragraph.

Group I—Three samples roughly overlap with AFT ages (1s) but the AHe single grain age dispersion is quite high and yields inverted AHe-AFT age correlation. This could result from, for example long residence in the PRZ or PAZ as suggested by the old ZFT ages. However, zoning or defects for underdispersion could not be identified as possible reasons for these results. Sample PK2 yields high reproducibility, with a mean AHe age of 14 Ma. As no acceptable or good paths from Southalpine samples could be modelled in HeFTy, a surface sample derived from Permian Brixen Granite, located almost exactly above sample PK1 was used instead (sample F1032 in Pomella, Stipp, & Fügenschuh, 2012).

±σ [Ma]	$Radius_{es}$ [µm]	U [ppm]	Th [ppm]	Sm [ppm]	^{4}He [nmol/g]	eU [ppm]	FT ^{238}U	FT ^{235}U	FT ^{232}Th	FT ^{147}Sm	Fully FT corr. Age ± 1σ [Ma]	Weighted mean Age[a] ±1σ [Ma]
0.56	33.27	19.84	59.85	556.71	2.11	33.91	0.59	0.54	0.54	0.87	19.58 ± 0.98	24.50 ± 0.45
0.40	41.89	27.45	42.66	616.49	3.87	37.48	0.67	0.62	0.62	0.89	28.40 ± 0.61	
0.54	32.70	14.53	26.52	341.57	1.31	20.76	0.59	0.53	0.53	0.86	19.88 ± 0.93	
0.34	40.10	19.83	38.32	653.47	1.35	28.84	0.65	0.61	0.61	0.89	13.09 ± 0.53	14.30 ± 0.29
0.35	44.51	16.31	26.48	413.94	1.24	22.53	0.69	0.64	0.64	0.90	14.70 ± 0.51	
0.29	37.53	37.19	58.45	715.41	2.60	50.93	0.63	0.59	0.59	0.88	14.92 ± 0.47	
0.53	39.67	18.61	40.11	480.41	3.12	28.04	0.65	0.61	0.61	0.89	31.47 ± 0.84	25.62 ± 0.50
0.45	40.39	17.86	28.89	420.98	1.61	24.65	0.66	0.61	0.61	0.89	18.31 ± 0.70	
0.80	33.00	8.81	16.93	312.83	1.56	12.79	0.59	0.54	0.54	0.86	37.75 ± 1.37	
0.15	34.89	43.11	16.87	107.36	0.93	47.07	0.61	0.56	0.56	0.87	6.04 ± 0.25	2.27 ± 0.04
0.03	64.86	84.43	20.32	135.66	0.78	89.21	0.78	0.75	0.75	0.93	2.08 ± 0.04	
0.11	85.52	18.55	4.94	85.56	0.27	19.71	0.83	0.80	0.80	0.95	3.09 ± 0.13	
0.07	39.77	38.48	28.49	242.59	0.14	45.18	0.65	0.61	0.61	0.89	0.86 ± 0.11	1.69 0.06
0.08	48.81	47.99	9.56	192.65	0.41	50.23	0.71	0.67	0.67	0.91	2.14 ± 0.12	
0.07	43.07	67.01	16.20	204.65	0.52	70.82	0.68	0.63	0.63	0.89	2.01 ± 0.10	
0.14	35.79	13.98	4.65	121.31	0.12	15.07	0.62	0.57	0.57	0.87	2.33 ± 0.23	2.76 0.20
0.36	43.62	20.37	3.97	114.66	0.29	21.31	0.68	0.64	0.64	0.90	3.75 ± 0.53	
0.66	50.11	13.17	15.30	119.28	0.45	16.77	0.72	0.68	0.68	0.91	6.91 ± 0.93	
0.06	83.45	118.54	27.05	261.82	2.11	124.90	0.82	0.80	0.80	0.94	3.81 ± 0.07	4.29 ± 0.04
0.08	91.26	110.81	17.35	218.98	3.01	114.88	0.84	0.82	0.82	0.95	5.78 ± 0.10	
0.06	148.26	60.34	43.71	327.45	1.39	70.61	0.90	0.88	0.88	0.97	4.05 ± 0.07	
0.09	71.93	68.77	67.42	232.37	2.00	84.61	0.80	0.77	0.77	0.94	5.51 ± 0.11	4.46 ± 0.06
0.09	65.69	88.43	70.18	262.41	2.08	104.92	0.78	0.75	0.75	0.93	4.73 ± 0.12	
0.08	66.13	38.90	33.18	226.16	0.67	46.69	0.78	0.75	0.75	0.93	3.41 ± 0.10	
0.05	79.27	74.03	90.08	283.15	1.30	95.20	0.82	0.79	0.79	0.94	3.12 ± 0.06	3.74 ± 0.04
0.08	96.70	51.59	44.95	200.55	1.28	62.15	0.85	0.83	0.83	0.95	4.52 ± 0.10	
0.07	85.52	60.11	57.17	206.95	1.48	73.55	0.83	0.80	0.80	0.94	4.50 ± 0.09	
0.07	50.25	66.46	86.97	136.50	1.65	86.89	0.72	0.68	0.68	0.91	4.95 ± 0.10	3.58 ± 0.07
0.07	50.76	64.27	101.08	133.83	0.65	88.02	0.72	0.68	0.68	0.91	1.93 ± 0.11	
0.08	74.04	45.98	56.97	120.34	0.63	59.36	0.69	0.65	0.65	0.90	2.90 ± 0.11	3.31 ± 0.07
0.07	47.11	83.97	83.12	154.83	1.46	103.50	0.72	0.69	0.69	0.91	3.64 ± 0.10	

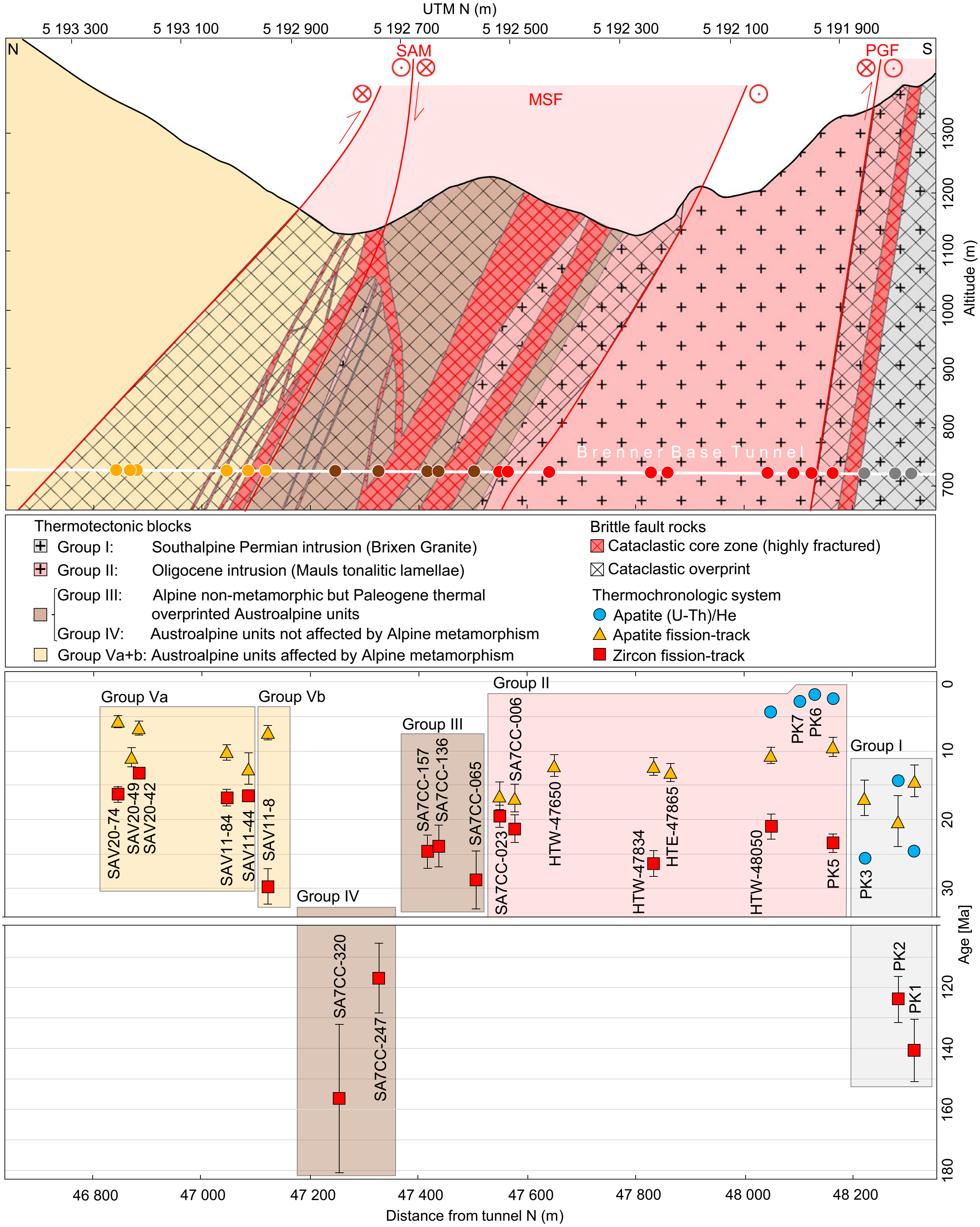

FIGURE 4 Sampling positions and age data along the sampled part of the BBT cross section within the fault rocks of the Periadriatic and Mauls-Sprechenstein fault systems. Note that ordinate axis Age [Ma] is plotted in two sections due to lack of ages between 35 and 100 Ma. Not every sample contained crystals suitable for all applied dating techniques (ZFT, AFT, AHe) and modelling of thermal histories [Colour figure can be viewed at wileyonlinelibrary.com]

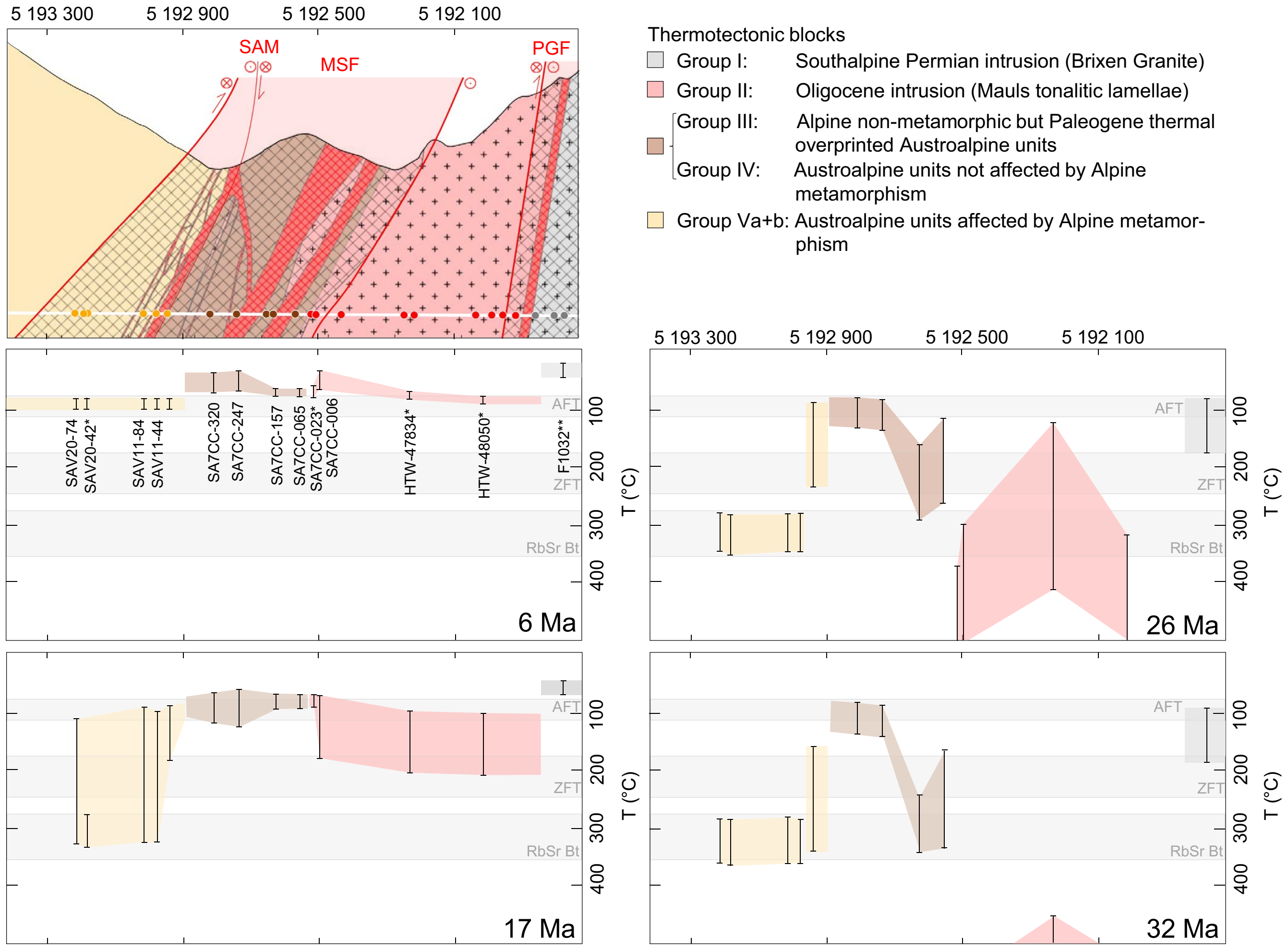

FIGURE 5 Visualization of thermochronologic data showing snap shots in time during Alpine orogeny, each significant for a state of regional tectonic evolution. Tunnel section and position of the samples are shown on the *x*-axis, whereas temperature is given on the *y*-axis. 32 Ma: The Mauls tonalitic lamellae starts to exhume after its emplacement, tectonically requiring a relative upward movement on both the northern and southern border. 26 Ma: Main phase of cooling in the Mauls tonalitic lamellae, most likely related to exhumation. The bend in temperature distribution within the Mauls tonalitic lamellae is conspicuous. 17 Ma: Differential uplift within the cross section right after incipient Giudicarie activity. Levelling out N and S SAM is conspicuous for this stage. The wide range of uncertainty for temperature and depth is noticeable. 6 Ma: Differential vertical movement is accommodated by the southern branch of the PGF and the SAM, which coincides with the DAV here *modelled path; **path modelled by Pomella et al. (2012) for sample F1032; all other samples could not be modelled and were fit to the paths of the proper modelled ones; for samples SA7CC-320 and SA7CC-320 cooling paths are straight as no modelling could be performed) [Colour figure can be viewed at wileyonlinelibrary.com]

TABLE 3 Number of samples and group age ranges

Group	ZFT ages #	ZFT age Range [Ma]	AFT ages #	AFT age Range [Ma]	AHe ages #	AHe age Range [Ma]
I	2	141–124	3	20–14	3	14–26
II	5	26–19	7	7–9	8	4.5–1.7
III	3	28–24	–	–	–	–
IV	2	156–117	–	–	–	–
Va	5	30	5	7	–	–
Vb	1	17–13	1	13–6	–	–

Group II—The AHe ages yield a high reproducibility. Modelling was based on samples SA7CC-023, HTW-48050 and HTW-47834.

Group IV—The ZFT age of sample SA7CC-320 was based on five single grain ages only, with a range between approximately 70 and 300 Ma it is over-dispersed. However, it is noteworthy

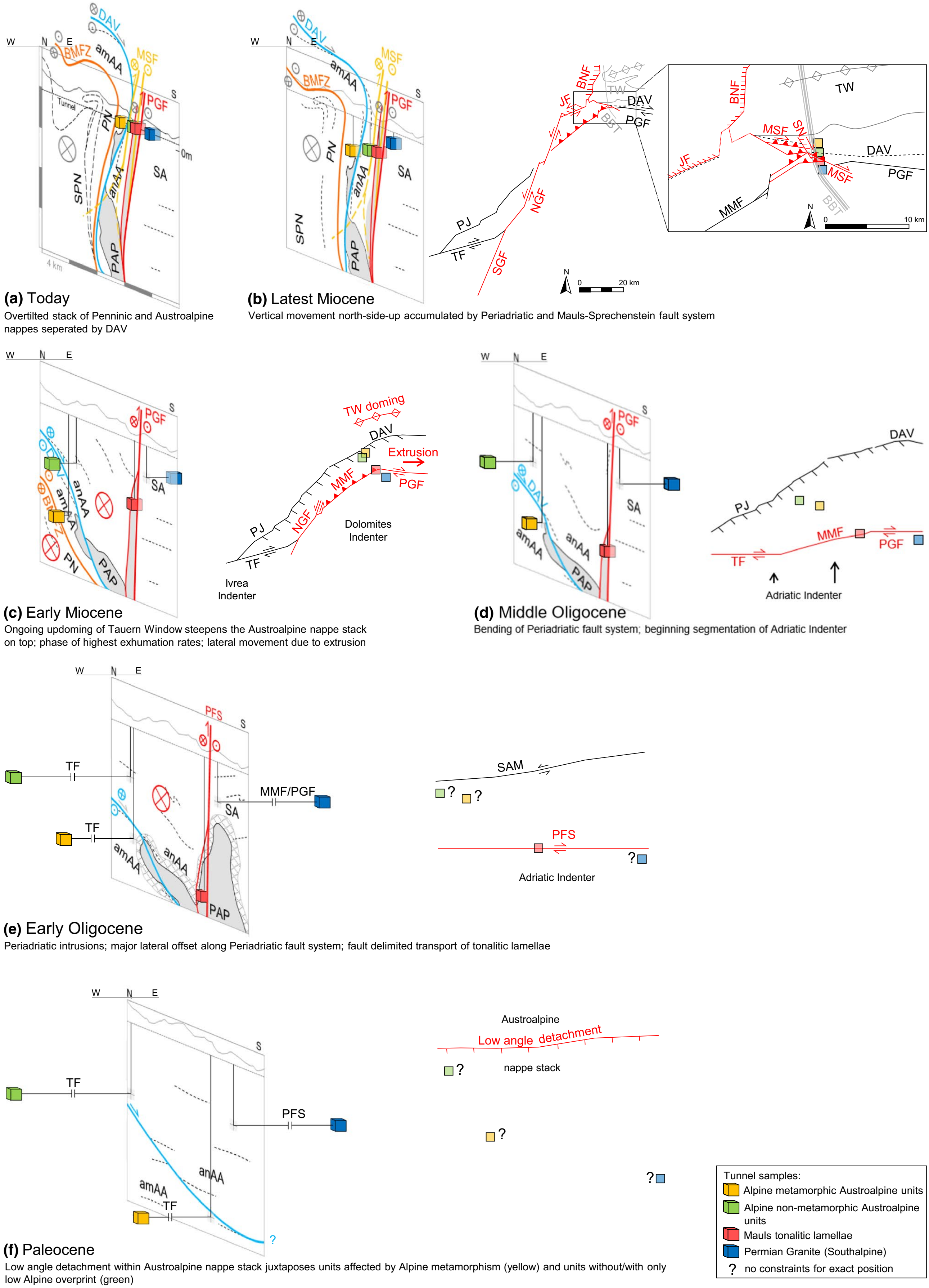

(a) Today
Overtilted stack of Penninic and Austroalpine nappes seperated by DAV

(b) Latest Miocene
Vertical movement north-side-up accumulated by Periadriatic and Mauls-Sprechenstein fault system

(c) Early Miocene
Ongoing updoming of Tauern Window steepens the Austroalpine nappe stack on top; phase of highest exhumation rates; lateral movement due to extrusion

(d) Middle Oligocene
Bending of Periadriatic fault system; beginning segmentation of Adriatic Indenter

(e) Early Oligocene
Periadriatic intrusions; major lateral offset along Periadriatic fault system; fault delimited transport of tonalitic lamellae

(f) Paleocene
Low angle detachment within Austroalpine nappe stack juxtaposes units affected by Alpine metamorphism (yellow) and units without/with only low Alpine overprint (green)

FIGURE 6 Compilation of main deformation stages connected to the tectonic evolution of the Tauern Window in cross section and map view, illustrated using present-day's position of the BBT cross section (Figure 3) and the tonalitic lamellae as a spatial reference; horizontal black lines illustrate lateral movement and cannot be scaled but give an indication of paleogeographic position (abbreviations attached provide information of fault segments that compensate next step lateral movement); Abbreviations see Figure 2 [Colour figure can be viewed at wileyonlinelibrary.com] [Correction added on 17 May 2019 after first online publication: Figure 6(d) has been updated.]

that no single grain was measured at a younger age than earliest Paleocene.

Group Vb—The over-dispersion of sample SAV11-8 is caused by two young grains.

Group Va—Sample SAV20-42 was used for a HeFTy modelling of the cooling path.

Group III and IV contained no apatite suitable for dating due to the intense cataclastic overprint. Within group Va + b apatite was present and suitable for AFT analysis but did not pass requirements for AHe dating.

5 | DISCUSSION

Our new cooling ages and paths constrain the timing of post-Cretaceous, Alpine processes at the boundary between the Eastern and Southern Alps. The results are discussed in time slices (Figure 5) of cooling behaviour to visualize differential movements during large-scale tectonic events.

We put special focus on the PGF, where differential vertical movement is only known for the strike-slip duplex of the Eder unit in the Carnian Alps (Läufer, Frisch, Steinitz, & Loeschke, 1997) and the Karawanken (positive) flower structure (Heberer et al., 2016; Nemes, 1996). Kinematics of the PGF's westernmost segment comprise dextral strike-slip and a north-side-up component during a late brittle stage (Mancktelow et al., 2001).

The following stages are derived from existing literature. However, our data constrain timing and occurrence of expected processes:

5.1 | Upper Cretaceous–Late Eocene: low angle detachment within the Austroalpine nappe stack

The step in ZFT data between Groups Va/b (Oligocene–Miocene) and IV (Mesozoic) clearly indicates the SAM in the presented cross section (Figures 4 and 6f). The presumable process driving the exhumation of Group Va/b is the partial collapse of the Eoalpine nappe stack (low-angle detachment during E–W extension in the Brenner region senso Fügenschuh, 1995). Late Cretaceous to early Paleocene extension along low-angle detachments in Austroalpine units was also described by Froitzheim et al. (1994). However, we cannot provide a well-constrained cooling path as strong cataclastic overprint severely decreased the number of countable apatite grains. The formerly south-directed extensional structures were incorporated in the steeply N-dipping, overtilted southern limb of the western Tauern sub-dome during Neoalpine updoming (Mancktelow et al., 2001; Stöckli, 1995).

Mancktelow et al. (2001) characterized the kinematics of the DAV as sinistral with a minor north-side-up component until the latest Eocene. Furthermore, Müller et al. (2001) presented ages from 60 to 25 Ma on synkinematic markers for DAV activity, such as $^{40}Ar/^{39}Ar$ on pseudotachylites and Rb/Sr on mica in mylonites, indicating a long-lasting, poly-phase activity of this structure. Biermeier and Krenn (1998) suggest a zone of enhanced deformation intensity between Rensen Tonalite and PGF as an eastward continuation of the DAV from our working area. For the DAV south of the Oligocene Rieserferner pluton further E, Wagner, Rosenberg, Handy, Möbus, and Albertz (2006) deduce syn- and post-emplacement DAV activity from preserved sinistral magmatic and solid-state foliations.

5.2 | Late Eocene–Oligocene: periadriatic intrusions and strike-slip movement along the PFS

Pomella et al. (2011) dated the Mauls lamellae using LA-ICP-MS U/Pb on zircon and report Oligocene intrusion ages (33–32 Ma) (Figure 6d,e). The intrusion depths of these plutonic rocks range from 5–12 km (Castellarin et al., 2005) up to 15–25 km in the Rensen area near Mauls (Trepmann, Stöckhert, & Chakraborty, 2004). We suggest the heat advection related to Periadriatic intrusions as a possible reason for Oligocene ZFT ages in Alpine non-metamorphic Austroalpine rocks (Group III). These ages are in the range of the adjacent Mauls lamellae (Group II). The extent of thermal reset has been quantified using the software 4DTherm (Fu & McInnes, 2006) which describes the cooling history of igneous bodies from their assumed emplacement temperature. Assuming a country rock temperature of <200°C, a rectangular shape (2 × 1 km) of the intrusion and a total exhumation of 4 km, it shows complete resetting of ZFT samples up to a distance of ca. 300 m from the intrusion.

5.3 | Miocene: Giudicarie fault activity, northward movement of Dolomites Indenter, main phase of Tauern Window compression

The data presented (Figures 4 and 6c) suggest differential vertical movement at the SAM (later cooling of Group Va/b compared to IV). This indicates that a successor of the DAV is still active in Miocene. Time-temperature paths (Supporting Information) derived from the Austroalpine unit north of the SAM (Group Va) indicate fastest cooling from 18 to 9 Ma. This step represents the main exhumation pulse which almost compensates the temperature difference between today's adjacent Austroalpine units (Figure 5). The temperature step across the PGF between Group I and II is still noticeable.

5.4 | Late Miocene–today: ongoing backthrusting

Top-to-south, brittle reverse faults, kink bands and folds (Figure 6a,b), interpreted as backthrusts related to ongoing indentation, were mapped by Stöckli (1995) and Mancktelow et al. (2001). These are the structures which most likely accommodate the north-side-up movement indicated by our data. They crosscut all structures except the top-to-east normal faults (Figure 3) and therefore indicate a very late stage in orogenic compression.

For the Karawanken mountains, Heberer et al. (2016) indicate a shift from confined exhumation in the Tauern Window and its surrounding nappes to a more widespread exhumation including parts of the Dolomites Indenter, that is the Valsugana and Val Trompia thrusts, from late Miocene onwards. AHe ages within the southernmost Austroalpine units and magmatic belts of the Karawanken Mountains north of the PGF range from 13 to 3 Ma.

Pliocene to Pleistocene AHe ages of the Mauls tonalitic lamellae (Group II: 4.5–1.7 Ma) and middle Miocene ages in the Southalpine Permian Granite (Group I) attest a relevant vertical displacement on the PGF from late Neogene time onwards. Aforementioned top-to-south thrusts (Mancktelow et al., 2001) are most likely assigned to this tectonic phase.

6 | CONCLUSIONS

New AHe, AFT and ZFT data based on samples derived from the Brenner Base Tunnel and modelled time-temperature paths allow for the following conclusions:

The narrow Austroalpine corridor near Mauls accommodates a significant amount of vertical displacement.

Younger AFT and AHe ages north of the PGF indicate north-side-up movement in the Miocene. Thus, the PGF (i) is not a pure strike-slip fault but has an important north-side up kinematic and (ii) was active at least until Pliocene times.

A striking change in ZFT ages localises the position of the Southern limit of Alpine metamorphism within the narrow, overtilted Austroalpine nappe stack and confirms Miocene activity at the DAV.

ACKNOWLEDGEMENTS

We acknowledge support by the Brenner Basistunnel BBT SE and are especially grateful for Ulrich Burger's counseling. All tunnel samples and a basic version of the cross section were kindly provided. Matteo Massironi supported the authors with valuable input during discussion. We thank Andrea Eberhöfer for the preparation of the samples. The University of Innsbruck provided student scholarship funding.

DATA AVAILABILITY

The data that support the findings of this study are presented in Tables 1 and 2. Thermal history models are available from the corresponding author.

ORCID

Thomas Klotz https://orcid.org/0000-0001-6187-229X
Hannah Pomella https://orcid.org/0000-0002-7695-4121
Martin Reiser https://orcid.org/0000-0002-8077-7893
Massimiliano Zattin https://orcid.org/0000-0002-2265-3921

REFERENCES

Becke, F. (1903). Exkursion durch das Westende der Hohen Tauern (Zillertal). *Führer Für Geologische Exkurisonen in Österreich, Internationale Geologische Konferenz*, *9*, 1–41.

Bertrand, A., Rosenberg, C., Rabaute, A., Herman, F., & Fügenschuh, B. (2017). Exhumation mechanisms of the Tauern Window (Eastern Alps) inferred from apatite and zircon fission-track thermochronology: Exhumation of the Tauern Window. *Tectonics*, *36*, 207–228.

Bianchi, A., Callegari, E., & Jobstraibizer, P. G. (1970). *I tipi petrografici fondamentali del Plutone dell'Adamello. Tonaliti, quarzdioriti, granodioriti e loro varietà leucocrate*. Padova, Italy: Societa Cooperativa Tipografica.

Biermeier, C., & Krenn, K. (1998). *Strukturgeologische Untersuchungen der oligozänen Rensen Intrusion und ihrer Rahmengesteine (Oberes Valstal, Südtirol)*. Unpublished Diploma Thesis, University of Graz.

Bistacchi, A., Massironi, M., & Menegon, L. (2010). Three-dimensional characterization of a crustal-scale fault zone: The Pusteria and Sprechenstein fault system. *Journal of Structural Geology*, *32*, 2022–2041. https://doi.org/10.1016/j.jsg.2010.06.003

Bögel, H. (1975). Zur Literatur über die "Periadriatische Naht". *Verhandlungen der Geologischen Bundesanstalt*, *2–3*, 163–199.

Borsi, S., Del Moro, A., & Ferrara, G. (1972). Età radiometriche delle rocce intrusive del Massiccio di Bressanone-Ivigna-Monte Croce (Alto Adige). *Bollettino della Società Geologica Italiana*, *91*, 387–406.

Brandner, R. (1980). Geologische Übersichtskarte von Tirol. In *Tirol-Atlas*. Innsbruck, Austria: Universitätsverlag Wagner.

Brandner, R., Reiter, F., & Töchterle, A. (2008). Überblick zu den Ergebnissen der geologischen Vorerkundung für den Brenner-Basistunnel. *Geography of the Alps*, *5*, 165–174.

Carlson, W. D., Donelick, R. A., & Ketcham, R. A. (1999). Variability of apatite fission-track annealing kinetics: I. Experimental Results. *American Mineralogist*, *84*, 1213–1223. https://doi.org/10.2138/am-1999-0901

Castellarin, A., Nicolich, R., Fantoni, R., Cantelli, L., Sella, M., & Selli, L. (2005). Structure of the lithosphere beneath the Eastern Alps (southern sector of the TRANSALP transect). *Tectonophysics*, *414*, 1–24.

Dal Piaz, G. (1926). Il confine alpino-dinarico dall'Adamello al massiccio di Monte Croce nell'Alto Adige. *Atti Dell'accademia Scientifica Veneto-Trentino-Istriana*, *17*, 3–7.

Dal Piaz, G. (1942). Geologia della bassa Val d'Ultimo e del massiccio di Monte Croce con considerazioni sull'etá e la giacitura delle masse intrusive periadriatiche e sulla tettonica del bacino dell'Adige. *Memorie del Museo di Storia Naturale della Venezia Tridentina*, *5*, 179–360.

Deutsch, A. (1984). Young Alpine dykes south of the Tauern Window (Austria): A K-Ar and Sr isotope study. *Contributions to Mineralogy and Petrology*, *85*, 45–57. https://doi.org/10.1007/bf00380220

Donelick, R. A. (1993). Apatite etching characteristics versus chemical composition. *Nuclear Tracks and Radiation Measurements*, *21*, 604. https://doi.org/10.1016/1359-0189(93)90241-z

Donelick, R. A., Carlson, W. D., & Ketcham, R. A. (1999). Variability of apatite fission-track annealing kinetics: II. Crystallographic orientation results. *American Mineralogist*, *84*, 1224–1234. https://doi.org/10.2138/am-1999-0902

Frisch, W. (1977). Der alpidische Internbau der Venedigerdecke im westlichen Tauernfenster. *Neues Jahrbuch Geologische und Paläontologische Monatshefte*, *11*, 675–696.

Frisch, W., Kuhlemann, J., Dunkl, I., & Brügel, A. (1998). Palinspastic reconstruction and topographic evolution of the Eastern Alps during late Tertiary tectonic extrusion. *Tectonophysics*, *297*, 1–15. https://doi.org/10.1016/s0040-1951(98)00160-7

Froitzheim, N., Schmid, S. M., & Conti, P. (1994). Repeated change from crustal shortening to orogen-parallel extension in the Austroalpine units of Graubünden. *Eclogae Geologicae Helvetiae*, *87*, 559–612.

Froitzheim, N., Schmid, S. M., & Frey, M. (1996). Mesozoic paleogeography and the timing of eclogite metamorphism in the Alps: A working hypothesis. *Eclogae Geologicae Helvetiae*, *89*, 81–110.

Fu, F., & McInnes, B. I. A. (2006). 4DTHERM: Constraining thermal and exhumation histories of magmatic-hydrothermal systems using U-Pb and (U–Th)/He data. *Geochmica et Cosmochimica Acta*, *70*, A412. https://doi.org/10.1016/j.gca.2006.06.830

Fügenschuh, B. (1995). *Thermal and kinematic history of the Brenner area (Eastern Alps, Tyrol)* (225 p). Disertation, Zürich, Switzerland: ETH Zürich.

Handy, M. R., Schmid, S. M., Bousquet, R., Kissling, E., & Bernoulli, D. (2010). Reconciling plate-tectonic reconstructions of Alpine Tethys with the geological–geophysical record of spreading and subduction in the Alps. *Earth-Science Reviews*, *102*, 121–158. https://doi.org/10.1016/j.earscirev.2010.06.002

Handy, M. R., Ustaszewski, K., & Kissling, E. (2015). Reconstructing the Alps–Carpathians–Dinarides as a key to understanding switches in subduction polarity, slab gaps and surface motion. *International Journal of Earth Sciences*, *104*, 1–26. https://doi.org/10.1007/s00531-014-1060-3

Hansmann, W., & Oberli, F. (1991). Zircon inheritance in an igneous rock suite from the southern Adamello batholith (Italian Alps). *Contributions to Mineralogy and Petrology*, *107*, 501–518. https://doi.org/10.1007/bf00310684

Heberer, B., Reverman, R. L., Fellin, M. G., Neubauer, F., Dunkl, I., Zattin, M., … Brack, P. (2016). Postcollisional cooling history of the Eastern and Southern Alps and its linkage to Adria indentation. *International Journal of Earth Sciences*, *106*, 1557–1580. https://doi.org/10.1007/s00531-016-1367-3

Hoinkes, G., Koller, F., Rantitsch, G., Dachs, E., Höck, V., Neubauer, F., & Schuster, R. (1999). Alpine metamorphism of the Eastern Alps. *Schweizerische Mineralogische und Petrographische Mitteilungen*, *79*, 155–181.

Hurford, A. J., & Green, I. R. (1983). The zeta age calibration of fission track dating. *Isotope Geoscience*, *1*, 285–317. https://doi.org/10.1016/s0009-2541(83)80026-6

Ketcham, R. A. (2005). Forward and inverse modeling of low-temperature thermochronometry data. *Reviews in Mineralogy and Geochemistry*, *58*, 275–314. https://doi.org/10.2138/rmg.2005.58.11

Ketcham, R. A., Carter, A., Donelick, R. A., Barbarand, J., & Hurford, A. J. (2007). Improved modeling of fission-track annealing in apatite. *American Mineralogist*, *92*, 799–810. https://doi.org/10.2138/am.2007.2281

Lammerer, B. (1988). Thrust-regime and transpression regime tectonics in the Tauern Window (Eastern Alps). *Geologische Rundschau*, *77*, 143–156. https://doi.org/10.1007/bf01848681

Lammerer, B., & Weger, M. (1998). Footwall uplift in an orogenic wedge: The Tauern Window in the Eastern Alps of Europe. *Tectonophysics*, *285*, 213–230. https://doi.org/10.1016/s0040-1951(97)00272-2

Laubscher, H. P. V. (1971). Das Alpen-Dinariden-Problem und die Palinspastik der südlichen Tethys. *International Journal of Earth Sciences*, *40*, 813–833.

Läufer, A. L., Frisch, W., Steinitz, G., & Loeschke, J. (1997). Exhumed faultbounded Alpine blocks along the Periadriatic lineament: The Eder unit (Carnic Alps, Austria). *Geologische Rundschau*, *86*, 612–626. https://doi.org/10.1007/s005310050167

Linzer, H. G., Decker, K., Peresson, H., Dell'Mour, R., & Frisch, W. (2002). Balancing lateral orogenic float of the Eastern Alps. *Tectonophysics*, *354*, 211–237. https://doi.org/10.1016/s0040-1951(02)00337-2

Luth, S. W., & Willingshofer, E. (2008). Mapping of the post-collisional cooling history of the Eastern Alps. *Swiss Journal of Geosciences*, *101*, 207–223. https://doi.org/10.1007/s00015-008-1294-9

Mancktelow, N. S., Stöckli, D. F., Grollimund, B., Müller, W., Fügenschuh, B., Viola, G., … Villa, I. M. (2001). The DAV and Periadriatic fault system in the Eastern Alps south of the Tauern window. *International Journal of Earth Sciences*, *90*, 593–622.

Müller, W., Prosser, G., Mancktelow, N., Villa, I., Kelley, S., Viola, G., … Neubauer, F. (2001). Geochronological constraints on the evolution of the Periadreatic Fault System (Alps). *International Journal of Earth Sciences*, *90*, 623–653. https://doi.org/10.1007/s005310000187

Nemes, F. (1996). *Kinematics of the Periadriatic fault in the Eastern Alps—Evidence from structural analysis, fission track dating and basin modelling*. Salzburg, Austria: University of Salzburg.

Ortner, H., Reiter, F., & Brandner, R. (2006). Kinematics of the Inntal shear zone–sub-Tauern ramp fault system and the interpretation of the TRANSALP seismic section, Eastern Alps. *Austria Tectonophysics*, *414*, 241–258. https://doi.org/10.1016/j.tecto.2005.10.017

Pleuger, J., Mancktelow, N., Zwingmann, H., & Manser, M. (2012). K-Ar dating of synkinematic clay gouges from Neoalpine faults of the Central Western and Eastern Alps. *Tectonophysics*, *550*, 1–16. https://doi.org/10.1016/j.tecto.2012.05.001

Pomella, H., Flöss, D., Speckbacher, R., Tropper, P., & Fügenschuh, B. (2016). The western end of the Eoalpine High-Pressure Belt (Texel unit, South Tyrol/Italy). *Terra Nova*, *28*, 60–69. https://doi.org/10.1111/ter.12191

Pomella, H., Klötzli, U., Scholger, R., Stipp, M., & Fügenschuh, B. (2011). The Northern Giudicarie and the Meran-Mauls fault (Alps, Northern Italy) in the light of new paleomagnetic and geochronological data from boudinaged Eo-/Oligocene tonalites. *International Journal of Earth Sciences*, *100*, 1827–1850. https://doi.org/10.1007/s00531-010-0612-4

Pomella, H., Stipp, M., & Fügenschuh, B. (2012). Thermochronological record of thrusting and strike-slip faulting along the Giudicarie Fault System (Alps, Northern Italy). *Tectonophysics*, *579*, 118–130. https://doi.org/10.1016/j.tecto.2012.04.015

Ratschbacher, L., Frisch, W., Linzer, H. G., & Merle, O. (1991). Lateral extrusion in the Eastern Alps, part 2: Structural analysis. *Tectonics*, *10*, 257–271. https://doi.org/10.1029/90tc02623

Reiter, F., Freudenthaler, C., Hausmann, H., Ortner, H., Lenhardt, W., & Brandner, R. (2018). Active seismotectonic deformation in front of the Dolomites Indenter Eastern Alps. *Tectonics*, *37*, 4625–4654. https://doi.org/10.1029/2017tc004867

Rosenberg, C. L. (2004). Shear zones and magma ascent: A model based on a review of the Tertiary magmatism in the Alps. *Tectonics*, *23*, 1–21.

Rosenberg, C., Brun, J. P., Cagnard, F., & Gapais, D. (2007). Oblique indentation in the Eastern Alps: Insights from laboratory experiments. *Tectonics*, *26*, 1–23.

Rosenberg, C., Schneider, S., Scharf, A., Bertrand, A., Hammerschmidt, K., Rabaute, A., & Brun, J.-P. (2018). Relating collisional kinematics to exhumation processes in the Eastern Alps. *Earth-Science Reviews*, *176*, 311–344. https://doi.org/10.1016/j.earscirev.2017.10.013

Rottura, A., Bargossi, G. M., Caggianelli, A., Del Moro, A., Visonà, D., & Tranne, C. A. (1998). Origin and significance of the Permian high-K calc-alkaline magmatism in the central-eastern Southern Alps, Italy. *Lithos*, *45*, 329–348. https://doi.org/10.1016/s0024-4937(98)00038-3

Sassi, P. F., & Zanferrari, A. (1971). Osservazioni sulla granodiorite affiorante lungo la linea della Gail presso Hollbruck (Tirolo Orientale, Austria). *Studi Trentini di Scienze Naturali*, *48*, 271–281.

Sassi, P. F., & Zanferrari, A. (1973). Sulla presenza di una massa tonalitica lungo la linea della Gail fra Obertillach e Liesing (Austria). *Bollettino della Società Geologica Italiana*, *92*, 605–620.

Schmid, S. M., Aebli, H. R., & Zingg, A. (1989). The role of the Periadriatic Line in the tectonic evolution of the Alps. *Geological Society Special Publication*, *45*, 153–171. https://doi.org/10.1144/gsl.sp.1989.045.01.08

Schmid, S. M., Scharf, A., Handy, M. R., & Rosenberg, C. L. (2013). The Tauern Window (Eastern Alps, Austria): A new tectonic map, with cross-sections and a tectonometamorphic synthesis. *Swiss Journal of Geosciences*, *106*, 1–32. https://doi.org/10.1007/s00015-013-0123-y

Schneider, S., Hammerschmidt, K., Rosenberg, C. L., Gerdes, A., Frei, D., & Bertrand, A. (2015). U-Pb ages of apatite in the western Tauern Window (Eastern Alps): Tracing the onset of collision-related exhumation in the European plate. *Earth and Planetary Science Letters*, *418*, 53–65.

Selverstone, J. (1988). Evidence for east-west crustal extension in the eastern Alps: Implications for the unroofing history of the Tauern window. *Tectonics*, *7*, 87–105. https://doi.org/10.1029/tc007i001p00087

Stöckli, D. F. (1995). *Tectonics SW of the Tauern Window (Mauls area, Südtirol)* (270 p.). Diploma thesis, ETH, Zürich, Switzerland.

Thöni, M., & Jagoutz, E. (1993). Isotopic constraints for eo-Alpine high-P metamorphism in the Austroalpine nappes of the Eastern Alps: Bearing on Alpine olrogenesis. *Schweizerische Mineralogische und Petrographische Mitteilungen*, *73*, 177–189.

Thöny, W. F. (2008). *Permian contact metamorphism in the Southern Alpine*. Dissertation, University of Innsbruck, Innsbruck, Austria.

TRANSALP Working Group. (2002, correction published 2006). First deep seismic reflection images of the Eastern Alps reveal giant crustal wedges and transcrustal ramps. *Geophysical Research Letters*, *29*, 92/91–92/93.

Trepmann, C., Stöckhert, B., & Chakraborty, S. (2004). Oligocene trondhjemitic dikes in the Austroalpine basement of the Pfunderer Berge, Südtirol – Level of emplacement and metamorphic overprint. *European Journal of Mineralogy*, *16*, 641–659. https://doi.org/10.1127/0935-1221/2004/0016-0641

Trümpy, R. (1973). The timing of orogenic events in the Central Alps. In K. A. De Jong, & R. Scholten (Eds.), *Gravity and Tectonics* (pp. 229–252). New York, NY: Wiley.

Viola, G., Mancktelow, N. S., & Seward, D. (2001). Late Oligocene-Neogene evolution of Europe-Adria collision: New structural and geochronological evidence from the Giudicarie fault system (Italian Eastern Alps). *Tectonics*, *20*, 999–1020.

Viola, G., Mancktelow, N., Seward, D., Meier, A., & Martin, S. (2003). The Pejo fault system: An example of multiple tectonic activity in the Italian Eastern Alps. *Geological Society of America Bulletin*, *115*, 515–532. https://doi.org/10.1130/0016-7606(2003)115<0515:tpfsae>2.0.co;2

von Blanckenburg, F., Kagami, H., Deutsch, A., Oberli, F., Meier, M., Wiedenbeck, M., … Vai, G. B. (1998). The origin of Alpine plutons along the Periadriatic Lineament. *Schweizerische Mineralogische und Petrographische Mitteilungen*, *78*, 55–66.

Wagner, G. A., & van den Haute, P. (1992). *Fission-track dating*. Stuttgart, Germany: Enke.

Wagner, R., Rosenberg, C. L., Handy, M. R., Möbus, C., & Albertz, M. (2006). Fracture-driven intrusion and upwelling of a mid-crustal pluton fed from a transpressive shear zone – The Rieserferner Pluton (Eastern Alps). *Geological Society of America Bulletin*, *118*, 219–237. https://doi.org/10.1130/b25842.1

Werling, E. (1992). *Tonale-, Pejo- und Judicarien-Linie: Kinematik, Mikrostrukturen und Metamorphose von Tektoniten aus räumlich interferierenden aber verschiedenaltrigen Verwerfungszonen* (276 p.). Zürich, Switzerland: ETH.

Wolf, R., Farley, K., & Silver, L. (1996). Helium diffusion and low-temperature thermochronometry of apatite. *Geochimica et Cosmochimica Acta*, *60*, 4231–4240. https://doi.org/10.1016/s0016-7037(96)00192-5

SUPPORTING INFORMATION

Additional supporting information may be found online in the Supporting Information section at the end of the article.

How to cite this article: Klotz T, Pomella H, Reiser M, Fügenschuh B, Zattin M. Differential uplift on the boundary between the Eastern and the Southern European Alps: Thermochronologic constraints from the Brenner Base Tunnel. *Terra Nova*. 2019;31:281–294. https://doi.org/10.1111/ter.12398